Electron-impact excitation of the $(5d^{10}6s)^2S_{1/2} \rightarrow (5d^9 6s^2)^2D_{5/2,3/2}$ transitions in gold atoms

O. Zatsarinny and K. Bartschat
Department of Physics and Astronomy, Drake University, Des Moines, Iowa 50311, USA

M. Maslov, M. J. Brunger, and P. J. O. Teubner
ARC Centre for Antimatter-Matter Studies, School of Chemistry, Physics and Earth Sciences, Flinders University, G.P.O. Box 2100, Adelaide 5001, Australia

(Received 27 August 2008; published 29 October 2008)

Results from a joint experimental and theoretical investigation of electron-impact excitation of the $(5d^{10}6s)^2S_{1/2} \rightarrow (5d^9 6s^2)^2D_{5/2,3/2}$ transitions in gold atoms are presented. The relative experimental data are normalized to theoretical predictions obtained in a fully relativistic *B*-spline *R*-matrix (close-coupling) method. There is generally good agreement between the measured and predicted energy dependence of the integral cross section, although some discrepancies remain in the near-threshold maximum of the excitation function for the $(5d^9 6s^2)^2D_{3/2}$ state.

DOI: 10.1103/PhysRevA.78.042713 PACS number(s): 34.80.Dp

I. INTRODUCTION

In a recent publication [1], we reported the results of a joint experimental and theoretical investigation concerning electron-impact excitation of the $(5d^{10}6s)^2S_{1/2} \rightarrow (5d^{10}6p)^2P_{1/2,3/2}$ resonance transitions in gold atoms. As pointed out in that paper, a detailed knowledge of this process in general, and not restricted to resonance transitions alone, is of great importance for modeling applications in atmospheric physics, astrophysics, and plasma physics, to name just a few. In addition, gold as a complex heavy atom can be expected to be an excellent candidate for testing theoretical predictions, which need to be based on fully relativistic approaches. Among those are the relativistic distorted-wave (RDW) approximation [2], the relativistic convergent close-coupling (RCCC) [3] method, and the relativistic Dirac *B*-spline *R*-matrix (DBSR) method [4], all of which were quite successful in describing the resonant excitation process, provided proper care was taken of the complications arising from the diffuse, though filled, 5*d* subshell in Au. In the RCCC model, for example, this was done through adding semiempirical one-body and two-body core-polarization terms to the Dirac-Fock static potential of the otherwise inert core, while the core-valence correlation was explicitly included in the DBSR calculation by the use of term-dependent, nonorthogonal orbital sets and the addition of target states with a $5d^9$ occupation to the close-coupling expansion.

The present work is an extension of our previous efforts, this time involving the $(5d^{10}6s)^2S_{1/2} \rightarrow (5d^9 6s^2)^2D_{5/2,3/2}$ transitions. Note that the $(5d^9 6s^2)D_{3/2}$ state of gold serves as the lower level of the 312.3-nm line in the gold vapor laser (GVL). Hence, a detailed knowledge of its connection to the ground state by collisions with low-energy electrons is of crucial importance for understanding the functioning of the GVL.

From a purely theoretical point of view, describing the optically forbidden $(5d^{10}6s)^2S_{1/2} \rightarrow (5d^9 6s^2)^2D_{5/2,3/2}$ transitions is expected to be even more challenging than the resonant excitation of the $(5d^{10}6p)^2P_{1/2,3/2}$ states from the $(5d^{10}6s)^2S_{1/2}$ ground state. Given the apparent, though still indirect, importance of the 5*d* subshell already for the resonant processes, having a change in the 5*d* occupation numbers directly between the initial and final states should highlight the role of this subshell even further. Also, looking at the dominant configurations $5d^{10}6s$ and $5d^9 6s^2$, one can expect a strong configuration dependence in both the 6*s* and 5*d* one-electron orbitals.

At the present time, neither the RDW nor RCCC method is applicable to the problem of interest to this paper, since their computational implementations do not allow for the opening of inner *d* subshells. In principle, the Dirac *R*-matrix program (DARC) [5] and its most recent extension to include a large number of pseudostates [6] could be used, but we are not aware of previous or planned calculations in the near future. In any case, the DBSR approach appears to be a very promising tool to tackle the problem, due to its great flexibility associated with the possibility of employing configuration and even term-dependent orbitals.

The principal motivation of the present work, therefore, is twofold: (i) to establish a set of experimental benchmark data that can be used for modeling applications and (ii) to use these data as a thorough test of the recently developed DBSR method. As a by-product, we will argue below that the test is sufficiently successful to put the relative experimental data, with a reasonable degree of confidence, on an *absolute* scale.

After a brief description of the apparatus, concentrating on the most important details for the present work (see [1] for more general information), the specifics of the computational model will be outlined. This is followed by the presentation and discussion of the results, as well as some conclusions.

II. EXPERIMENTAL APPARATUS AND MEASUREMENT TECHNIQUES

The experimental arrangement is shown in Fig. 1. A laser-induced fluorescence technique was used to study the excitation function for the $(5d^9 6s^2)^2D_{3/2}$ state. This state was chosen because it lies 2.658 eV above the ground state, and

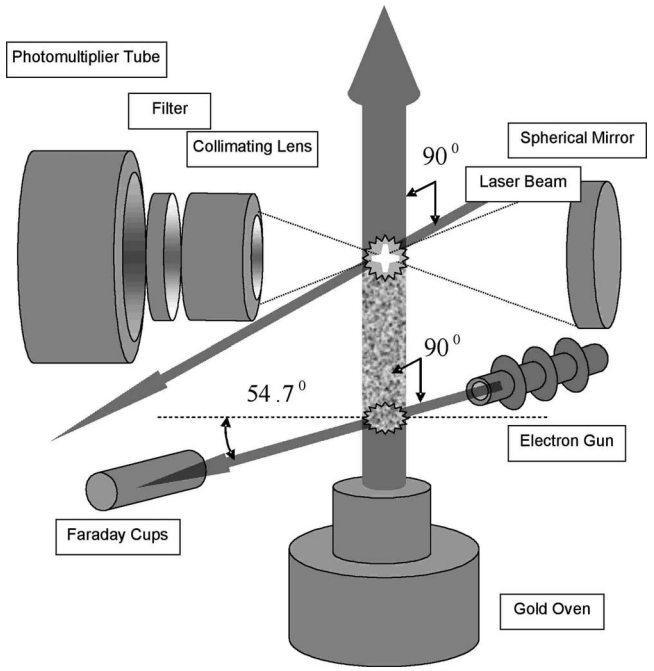

FIG. 1. Experimental configuration for the laser-induced fluorescence technique measurements.

thus its thermal population in the gold beam is negligible. Contrary to this, the thermal population of the $^2D_{5/2}$ state in the gold beam is very much larger than that which can be excited from the ground state by electron impact. Due to this thermal contamination, no measurement for the $^2D_{5/2}$ state was possible. A beam of gold atoms was produced by heating gold wire in a molybdenum crucible, which was heated to temperatures up to 1600 K by electron bombardment. Great care was taken to isolate the gold beam from these electrons. At this temperature the number density of gold atoms in the interaction region was about 4×10^{14} m^{-3}. The diameter of the gold beam was 7.5 mm, and its angular divergence was 0.12 rad [full width at half maximum (FWHM)]. The oven temperature was measured with a thermocouple, and the temperature was stabilized to 1 K over the course of the run by a feedback loop that controlled the electron emission as the oven temperature varied. The angular divergence of the beam resulted in a Doppler broadening of the $^2D_{3/2}\rightarrow{}^2P_{1/2}$ transition of 130 MHz (FWHM). While this value of the Doppler broadening is not germane to the present excitation function measurements, we include it here for completeness. The electron beam crossed the gold beam at right angles and was produced in a standard electrostatically focused electron gun.

The pump laser was introduced to the vacuum chamber through one of the side windows and intersected the atomic beam at an angle of 90°. This intersection point was several centimeters downstream from that between the electron and atomic beams. Note that the lifetime of the D state is such that at the mean speed of the gold atoms of 400 m/s there was negligible loss of D-state atoms at the laser site. The fluorescence was induced between the Hartree-Fock-Slater levels of the D and P states, and there was a choice of six possible transitions. We chose the $F=3$ to $F'=2$ transition between the D state and the $(5d^{10}6p)^2P_{1/2}$ state because this optimized the signal-to-noise ratio. The 627.8-nm laser light was generated in an argon-ion pumped ring dye laser operating on DCM dye.

Fluorescent photons from the $^2P_{1/2}$ state to the ground state at 267.6 nm were collected with a collimating lens, passed through an interference filter, and detected in a photomultiplier tube. A spherical mirror was mounted opposite to the lens, and its focus was contained within the laser atomic-beam interaction region. That mirror optimized the fluorescent light intensity. Note that care was taken in the experimental design to ensure that the measured florescence signal is indeed directly proportional to the collision cross section of interest. Provided that the $^2P_{1/2}$ resonant level can only spontaneously decay into the $^2S_{1/2}$ ground state (this is justified by the branching ratio being $R=0.98$ for that transition [7]), that no cascade contributions other than the small $^2P_{1/2}\rightarrow{}^2D_{3/2}$ cascade occur (this is satisfied by ensuring the upper incident electron energy limit is restricted to being less than 5.8 eV, which is below the nearest other cascade level), and that there are no interatomic collisions (this is satisfied as the mean free path of the Au atoms is ~600 mm with our Au beam densities, which is much larger than the linear dimensions of the interaction region), the rate equations for the $^2P_{1/2}$ and $^2D_{3/2}$ levels, under stationary conditions, reduce to [8]

$$F_{3/2}(E)=\frac{S_{\rm on}(E)-S_{\rm off}(E)}{I_e(E)}, \tag{1}$$

where $F_{3/2}(E)$ is the required excitation function, $S_{\rm on}$ and $S_{\rm off}$ are the measured decay fluorescence rates when the pump laser is on and off, and $I_e(E)$ is the incident electron-beam current. Note that the output from the photomultiplier tube was amplified and counted in one of two gated scalers. There were several sources of background in this experiment. In addition to what we discussed in a recent paper [1]—namely, the rise in the dark current caused by the increase in temperature inside the vacuum chamber—there was some contamination of the atomic beam caused by thermally excited D-state atoms. Another source of background was attributed to the scattering of laser light through the optical system. Therefore it was essential that both the laser beam and the electron beam were chopped.

The laser beam was chopped with a rotating wheel, which also generated a series of pulses that controlled the gates of the scalers. It was shown that the ratio for electron excitation of the $^2D_{3/2}$ state to thermal excitation was about 10 to 1.

III. COMPUTATIONAL METHOD

The numerical calculations for this work are based upon a fully relativistic DBSR method [4]. An important aspect, especially for a relatively complex target such as gold, is the *structure description*, which is by no means trivial. A particular difficulty in gold is the filled and very diffuse $5d$ subshell. While part of the Au spectrum consists of Rydberg-like $(\ldots5d^{10}nl)$ states, the two lowest excited states, which are the topic of this paper, have the dominant configuration $5d^96s^2$.

TABLE I. Calculated and observed [14] excitation energies for the Au states included in the ten-state (10CC) close-coupling expansion. Also given are the absolute energies (in atomic units) obtained in the structure calculation.

State	Theory (a.u.)	Theory (eV)	Experiment (eV)	Difference (eV)
$(5d^{10}6s)^2S_{1/2}$	−19035.617394	0.000	0.000	0.000
$(5d^96s^2)^2D_{5/2}$	−19035.575631	1.136	1.135	0.001
$(5d^96s^2)^2D_{3/2}$	−19035.519800	2.656	2.658	−0.002
$(5d^{10}6p)^2P_{1/2}$	−19035.447124	4.633	4.632	0.001
$(5d^{10}6p)^2P_{3/2}$	−19035.429500	5.113	5.105	0.008
$(5d^{10}7s)^2S_{1/2}$	−19035.365593	6.852	6.755	0.097
$(5d^{10}7p)^2P_{3/2}$	−19035.340119	7.545	7.443	0.102
$(5d^{10}7p)^2P_{3/2}$	−19035.337845	7.607	7.529	0.078
$(5d^{10}6d)^2D_{3/2}$	−19035.333516	7.725	7.681	0.044
$(5d^{10}6d)^2D_{5/2}$	−19035.333260	7.732	7.691	0.040

Hence one can expect a significant configuration dependence of the $5d$ and $6s$ orbitals.

The DBSR (close-coupling) approach is a newly developed extension of the BSR complex [9] to the fully relativistic Dirac scheme. It is described in detail in a recent application to e-Cs collisions [4]. The distinguishing features of the method are (i) the ability to use term-dependent, and hence nonorthogonal, sets of one-electron orbitals (Dirac spinors in the present case) in the target description and (ii) B-splines as the underlying, effectively complete basis to expand the wave function of the projectile. Furthermore, it is an all-electron approach, and hence core-valence correlation effects (such as the core polarization) can be described *ab initio*. As usual, the R-matrix method allows for an efficient calculation of results for a large number of collision energies, as needed particularly in near-threshold regimes that are often dominated by resonance structures. On the other hand, using a basis expansion for the projectile wave function limits the energy range to low and intermediate energies. It is also difficult to include a sufficient number of pseudostates to fully account for coupling to the ionization continuum, particularly for complex targets.

As mentioned previously, the low-energy spectrum of the gold atom consists of states with configurations $(5d^{10}nl)$, as well as core-excited states with configurations $(5d^96s^2)$ and $(5d^96s6p)$, respectively. For the first set, the principal correlation effects originate from the interaction of the valence electron with the core, whereas for the core-excited states the valence correlation itself is also important. The core-valence correlation was simulated by adding the $5d^9\bar{n}l\bar{n}'l'$ configurations, where the overbar indicates a correlated rather than a physical orbital. Different sets of correlated orbitals $\bar{n}l$ were optimized separately for the lowest state of each symmetry with target electronic angular momentum J. Since the mean radii for the $\bar{n}l$ orbitals lie between the mean radii of the core and valence orbitals, this method allows us to incorporate the core-valence correlation with a relatively small number of configurations.

We then considered the physical core-excited $(5d^96s^2)$ and $(5d^96s6p)$ states in separate multiconfiguration Dirac-Fock (MCDF) calculations. The expansions contained all configurations with promotion of two valence electrons to the set $\{6s,6p,6d,5f\}$. Note that we employed relaxed $5d$ and valence nl one-electron orbitals for the core-excited states. These orbitals, therefore, are not orthogonal to the corresponding orbitals in the $(5d^{10}nl)$ states. The relaxation effects were found to be very important in the present case, leading to corrections in the excitation energies of up to 1 eV. All the above calculations were carried out in the Dirac-Fock approximation using the GRASP2K relativistic atomic structure package [10].

Finally, the entire spectrum of Au was recalculated using the B-spline box-based expansion

$$\Phi(J\pi) = \mathcal{A}\{\varphi(5d^{10})\phi(nl)\} + a_i\varphi(5d^9\bar{n}l\bar{n}l') + b_i\varphi(5d^96s^2) + c_i\varphi(5d^96s6p), \tag{2}$$

where $\mathcal{A}$ denotes the antisymmetrization operator, J is the total electronic angular momentum of the target state, and π is the parity. Depending on the parity of the state of interest, either the $\varphi(5d^96s^2)$ (even) or $\varphi(5d^96s6p)$ (odd) configurations were allowed to mix in (2). The unknown large and small radial components for the outer valence electron, $\phi(nl)$, were expanded in separate B-spline bases as

$$P(r) = \sum_{i=1}^{n_p} p_i B_i^{k_p}(r), \tag{3}$$

$$Q(r) = \sum_{i=1}^{n_q} q_i B_i^{k_q}(r). \tag{4}$$

The coefficients of the B-spline expansions, p_i and q_i, together with the coefficients for the correlated and physical core-excited configurations, a_i, b_i, and c_i, were found by diagonalizing the Dirac-Coulomb Hamiltonian with the additional requirement that the wave functions vanish at the boundary. Note that we do not impose orthogonality of the valence orbitals nl to the correlated orbitals $\bar{n}l$ in the above procedure. This speeds up the convergence of the expansion (2) and yields accurate binding energies with a relatively small number (~50) of correlated configurations for each symmetry.

The number of physical states that we can generate in this method depends upon the size a of the R-matrix box. We chose $a=30a_0$, with $a_0=0.529\times10^{-10}$ m being the Bohr radius. This choice allowed us to obtain a good description for all low-lying Rydberg-type bound states of Au up to $n=8$. Along with these physical states, we also generated a set of pseudostates for each symmetry, with the lowest states representing the remaining bound states and the others representing the continuum. The resulting spectra also contain the core-excited states with configurations $(5d^96s^2)$ and $(5d^96s6p)$, respectively, some of which lie in the continuum. As seen from Table I, the resulting target excitation energies agreed with the experimental values at the level of 0.1 eV or better, including the $(5d^96s^2)^2D_{5/2,3/2}$ states. Note that all correlated orbitals employed were optimized on the lowest five states, individually for each state. As a result, the relative energies for the lowest states agree much better with experi-

TABLE II. Comparison of calculated and observed oscillator strengths for selected transitions in Au.

Transition	This work	RHF+CP [11]	Experiment [7]
$(6s)^2S_{1/2}\rightarrow(6p)^2P_{1/2}$	0.172	0.170	0.176 ± 0.003
$(6s)^2S_{1/2}\rightarrow(6p)^2P_{3/2}$	0.376	0.345	0.351 ± 0.015
$(5d^96s^2)^2D_{5/2}\rightarrow(6p)^2P_{3/2}$	0.015	0.011	0.018 ± 0.001
$(5d^96s^2)^2D_{3/2}\rightarrow(6p)^2P_{3/2}$	0.001	0.001	0.002 ± 0.001
$(5d^96s^2)^2D_{3/2}\rightarrow(6p)^2P_{3/2}$	0.004	0.002	0.010 ± 0.005

ment than those for the higher-lying states. The agreement for the $(5d^96s6p)$ states is less satisfactory, with the difference in the excitation energies between experiment and theory ranging from 0.1 to 0.5 eV. We did not include the core-valence correlation for these states, since it would require consideration of the $5d^8nln'l'n''l''$ configurations. This, in turn, would lead to a tremendous, currently unmanageable complication in the subsequent collision calculations. Note, however, that the $(5d^96s6p)$ states were only considered in order to check the convergence of our close-coupling expansion, and hence they have a less direct effect on the results presented below.

The oscillator strengths for the transitions between the lowest five states of Au are presented in Table II. Our values are in close agreement with the experimental data [7] and also with recent RHF+CV (relativistic Hartree-Fock plus core-polarization model potential) calculations [11]. As shown in a set of previous theoretical calculations (see, for example, Refs. [11,12]), both relativistic and core-polarization effects are extremely important to establish a reliable scale of f values for neutral Au and lead to corrections up to factors of 2. While most previous calculations accounted for such core-polarization effects through semiempirical potentials, we include these effects *ab initio* via the core-excited correlated configurations. The good agreement with the experimental data confirms the high accuracy of our approach.

In the present calculations, we used the Dirac-Coulomb Hamiltonian to describe both the N-electron target and the $(N+1)$-electron collision systems. The total wave function for each partial-wave symmetry was constructed from four-component Dirac spinors. Note that the radial functions for the large and small components were expanded in separate B-spline bases of different order. This allowed us to avoid the occurrence of pseudostates [13]. We used a semiexponential grid for the B-spline knot sequence and a relatively large number (150) of splines to cover the inner region up to the R-matrix radius of $30a_0$. This large number of splines was required to correctly describe the finite-size nuclear model, with a Fermi potential adopted in the present work.

In order to check the convergence of the close-coupling expansion, we performed several sets of scattering calculations with a different number of target states included. The initial close-coupling expansion contained ten target states with configurations $(5d^{10}6s,6p,7s,7p,6d)$ and $(5d^96s^2)$. We also carried out 15-state calculations, including five additional states with configurations $(5d^96s6p)$. These were chosen on the basis of having the largest oscillator strengths for dipole transitions from the $(5d^96s^2)$ states. Finally, we carried out a 32-state calculation, also including the physical $(5d^{10}8l)$ states and $(5d^{10}kl)$ pseudostates states (with $l=0,1,2$) lying in the target continuum. Partial-wave contributions up to a total electronic angular momentum of 15 for the collision system were calculated numerically. No top-up procedure was required to obtain partial-wave converged results for the transitions and energies under consideration. The cross sections, and any other scattering parameters of interest, were calculated in the same way as in the standard R-matrix approach.

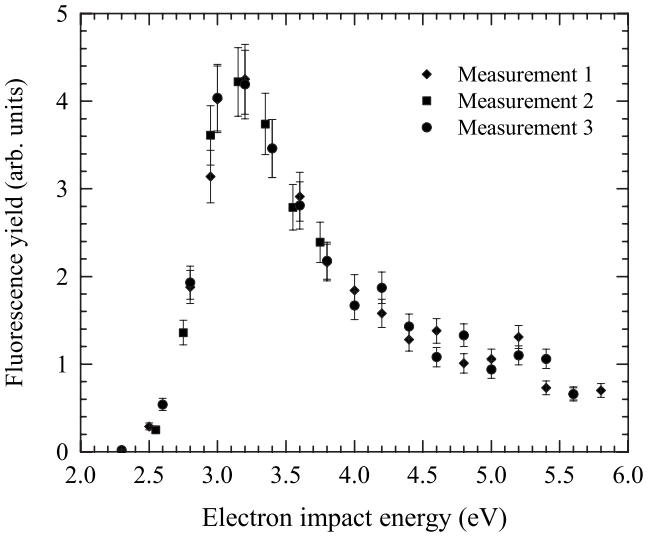

FIG. 2. Excitation function of the $(5d^96s^2)^2D_{3/2}$ state in gold. Shown are the relative experimental results obtained in three different runs.

IV. RESULTS AND DISCUSSION

The experimental fluorescence yield from three different measurements is shown in Fig. 2. We note that the measurements are confined to impact energies less than about 6 eV. The upper limit was set by the increasing significance of 267.6-nm photons arising from the direct excitation of the $P_{1/2}$ state. In principle, it is possible to normalize our D state cross section to the known P state cross section at a particular energy—e.g., 5 eV. In our case, however, we were unable to saturate the D state with the maximum laser power of 120 mW available to us. Consequently, only relative numbers are shown in this graph, but we indicate the level of reproducibility by plotting the data obtained in three different runs. This level of reproducibility is very good.

The theoretical results for the excitation function of both $(5d^96s^2)$ fine-structure states are shown in Fig. 3. In the upper panel, the predictions for the $(5d^96s^2)^2D_{3/2}$ state are compared with the average of the experimental data obtained in the different runs shown in Fig. 2. In this case, the experimental data were normalized to the presumably best theoretical prediction (32-state model) by a visual fit in the incident-energy range between 4 and 6 eV. Comparison of the theoretical results obtained with three different models, dis-

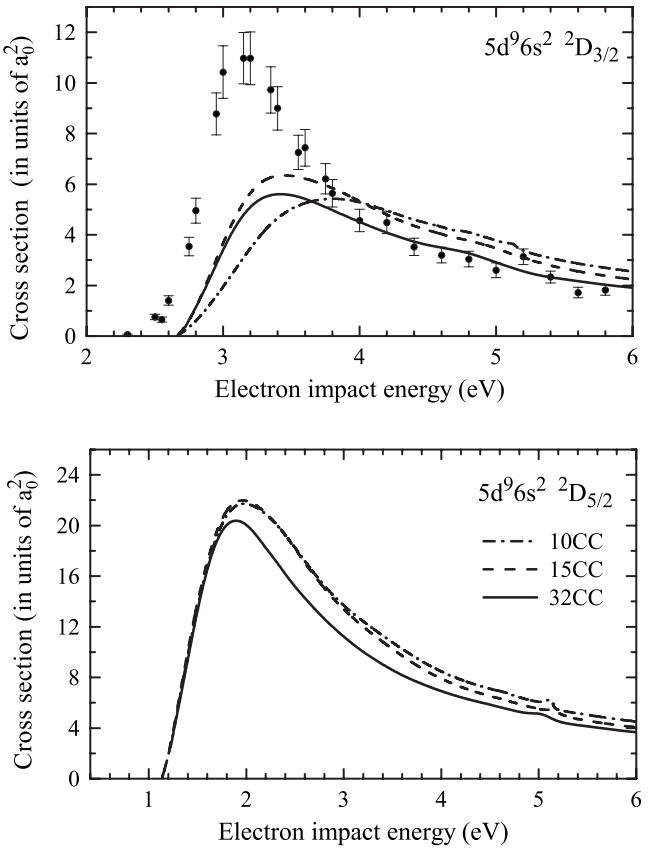

FIG. 3. Cross sections for electron impact excitation of the $(5d^96s^2)^2D_{5/3,3/2}$ states in gold. The experimental data in the top panel were visually normalized to the 32CC predictions in the energy range 4–6 eV (see text).

tinguished by the number of states included in the close-coupling expansion (see Sec. III for details), indicates a possibly slow convergence of the close-coupling expansion, particularly with respect to the position of the maximum. It is apparently very difficult to reproduce the measured shape of the excitation function. Interestingly, the predicted shape for the $(5d^96s^2)^2D_{5/2}$ level is much closer to the measurement for the $(5d^96s^2)^2D_{3/2}$ state than the theory for this state. At this point, we have no explanation for this most likely fortuitous finding, other than the convergence properties of the expansion. Unfortunately, currently available computational resources do not allow us to push these checks any further, and we do not expect this fact to change significantly in the foreseeable future.

Nevertheless, we believe that the agreement between experiment and theory is sufficiently good to put the experimental data on an absolute scale. Following well-established trends, including more states in the close-coupling expansion somewhat reduces the theoretical values for the excitation function outside the resonance region. Setting the absolute scale for the experimental data shown in the graph at an uncertainty of about 50% seems to be a conservative estimate. Table III lists the suggested absolute experimental values, obtained by averaging (if available) experimental data from different runs at the same energy and normalizing to theory as described above.

TABLE III. Suggested absolute experimental values for the electron impact excitation cross section of the $(5^{10}6s)^2S_{1/2} \rightarrow (5d^96s^2)^2D_{3/2}$ transition in gold. The uncertainties given are due to statistics and reproducibility. We estimate the absolute scale to be reliable within a factor of 2 (see text).

Energy (eV)	Cross section (a_0^2)
2.30	0.05 ± 0.03
2.50	0.75 ± 0.10
2.55	0.65 ± 0.10
2.60	1.40 ± 0.18
2.75	3.54 ± 0.36
2.80	4.95 ± 0.49
2.95	8.78 ± 0.83
3.00	10.43 ± 1.04
3.15	10.97 ± 1.01
3.20	10.97 ± 1.04
3.35	9.72 ± 0.91
3.40	9.00 ± 0.86
3.55	7.25 ± 0.68
3.60	7.44 ± 0.73
3.75	6.21 ± 0.60
3.80	5.64 ± 0.55
4.00	4.56 ± 0.44
4.20	4.49 ± 0.44
4.40	3.52 ± 0.34
4.60	3.20 ± 0.31
4.80	3.04 ± 0.31
5.00	2.60 ± 0.29
5.20	3.13 ± 0.31
5.40	2.33 ± 0.23
5.60	1.72 ± 0.21
5.80	1.82 ± 0.21

Comparing the theoretical results for the two fine-structure levels shows a strong violation of the statistical branching ratio (3:2 based on the relative weight factor proportional to $2J+1$). This is a clear indication for the need to treat this complicated problem in a fully relativistic manner. The theoretically predicted difference in the peak height is almost a factor of 4 between the $^2D_{5/2}$ and $^2D_{3/2}$ state, and the factor is still about 2 at 6 eV.

Finally, Fig. 4 displays the dominant partial-wave contributions to the excitation functions. Note that the broad maxima are due to different angular-momentum symmetries of the e-Au collision system: namely, $J=1^-$ for the $^2D_{3/2}$ state and $J=2^-$ for the $^2D_{5/2}$ state, respectively. In a nonrelativistic picture, both symmetries contain contributions from an incident p wave, with the f wave also contributing to $J=2^-$. Most interestingly, we see that only odd-parity symmetries, corresponding to incident and outgoing p and f waves, contribute significantly to the cross section. This suggests that the direct quadrupole-type $5d \rightarrow 6s$ one-electron transition process is much less important than the dipole-driven exchange process, in which an incident p or f con-

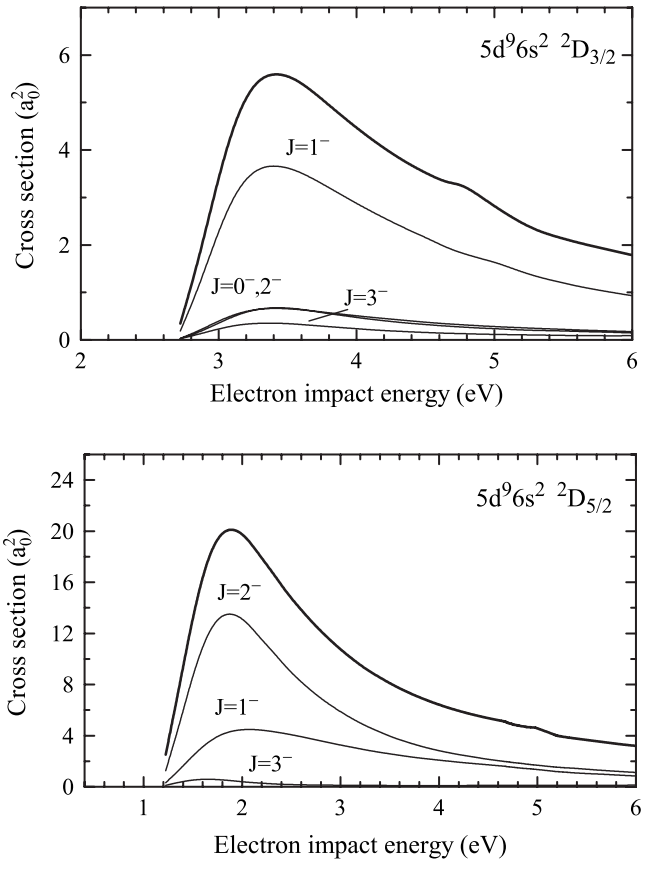

FIG. 4. Dominant partial-wave contributions to the excitation functions shown in Fig. 3. The thick lines represent the sums of the contributions, while the individual terms are labeled. Note that the $J=0^-$ and $J=2^-$ contributions are almost identical for the $^2D_{3/2}$ and hence hard to distinguish.

tinuum electron interacts with the active target electron in a complicated manner, ultimately leading again to a free electron with $l=1$ or $l=3$.

V. SUMMARY AND CONCLUSIONS

We have presented results from a joint experimental and theoretical study of electron impact excitation of the $(5d^{10}6s)^2S_{1/2} \rightarrow (5d^9 6s^2)^2D_{5/2,3/2}$ transitions in gold atoms. The calculations were performed using a newly developed, fully relativistic, and general *B*-spline *R*-matrix (close-coupling) code that allows for the treatment of complex atomic and ionic targets. In particular, relaxation effects in the one-electron orbitals and core-valence correlation can be treated *ab initio* and consistently in both the structure and the collision calculations. In spite of some remaining disagreements in the position and the relative height of the near-threshold maximum in the excitation function, the overall agreement between experiment gives us some confidence to put the experimental data on an absolute scale. Such absolute numbers are critical for the use of these data in modeling applications. We also hope that the current work will stimulate future efforts, both experimentally and theoretically, on this very challenging collision problem.

ACKNOWLEDGMENTS

This work was supported by the National Science Foundation (O.Z., K.B.) and by the Australian Research Council (M.M., M.J.B., P.J.O.T.). We thank Dr. Laurence Campbell for his assistance in the production of this paper.

[1] M. Maslov, M. J. Brunger, P. J. O. Teubner, O. Zatsarinny, K. Bartschat, D. V. Fursa, I. Bray, and R. P. McEachran, Phys. Rev. A **77**, 062711 (2008).
[2] V. Zeman, R. P. McEachran, and A. D. Stauffer, J. Phys. B **27**, 3175 (1994).
[3] D. V. Fursa and I. Bray, Phys. Rev. Lett. **100**, 113201 (2008).
[4] O. Zatsarinny and K. Bartschat, Phys. Rev. A **77**, 062701 (2008).
[5] S. Ait-Tahar, I. P. Grant, and P. H. Norrington, Phys. Rev. A **54**, 3984 (1996).
[6] N. R. Badnell, J. Phys. B **41**, 175202 (2008).
[7] P. Hannaford, P. L. Larkins, and R. M. Lowe, J. Phys. B **14**, 2321 (1981).
[8] M. S. Maslov, Ph.D. thesis, Flinders University, 2004.
[9] O. Zatsarinny, Comput. Phys. Commun. **174**, 273 (2006).
[10] P. Jönsson, X. He, C. Froese Fischer, and I. P. Grant, Comput. Phys. Commun. **177**, 597 (2007).
[11] V. Fivet, P. Quinet, É. Biémont, and H. L. Xu, J. Phys. B **39**, 3587 (2006).
[12] J. Migdalek and M. Garmulewicz, J. Phys. B **33**, 1735 (2000).
[13] C. Froese Fischer and O. Zatsarinny, e-print arXiv:0806.3116.
[14] C. E. Moore, *Atomic Energy Levels*, Natl. Bur. Stand. (U.S.) Circ. No. NSRDS-NBS 35 (U.S. GPO, Washington, DC, 1971), Vol. 3.